Joshi Manoj (Orcid ID: 0000-0002-2948-2811)
Johnson Martin (Orcid ID: 0000-0002-4706-8294)

A capacitor-discharge mechanism to explain the timing of orogeny-related global glaciations

Manoj M. Joshi*[1, 2], Benjamin J. W. Mills[3] and Martin Johnson[2,4]

[1]Climatic Research Unit, University of East Anglia, Norwich, UK

[2]Centre for Ocean and Atmospheric Sciences, University of East Anglia, Norwich, UK

[3]School for Earth and Environment, University of Leeds, Leeds, UK

[4]Bantry Marine Research Station, Gearhies, Bantry, Republic Of Ireland

***Corresponding Author Address**

M. Joshi, School of Environmental Sciences, University of East Anglia, Norwich Research Park, Norwich, NR4 7TJ, UK. Email: m.joshi@uea.ac.uk

Key Points

- A multimillion-year delay appears to exist between peaks in low-latitude mountain uplift and the maximum extent of Phanerozoic glaciation
- We describe a mechanism to explain the delay using a combination of climate and geochemical modelling of the periods surrounding uplift
- The mechanism suggests such a scenario potentially happening 10-50 million years in the future.

This article has been accepted for publication and undergone full peer review but has not been through the copyediting, typesetting, pagination and proofreading process which may lead to differences between this version and the Version of Record. Please cite this article as doi: 10.1029/2019GL083368

Abstract

Over geological timescales, mountain building or orogenesis is associated with increased weathering, the drawdown of atmospheric CO_2, and global cooling. However, a multimillion-year delay appears to exist between peaks in low-latitude mountain uplift and the maximum extent of Phanerozoic glaciation, implying a more complex causal relationship between the two. Here we show that global silicate weathering can be modulated by orogeny in three distinct phases. High, young mountain belts experience preferential precipitation and the highest erosion. As mountains are denuded, precipitation decreases, but runoff temperature rises, sharply increasing chemical weathering potential and CO_2 drawdown. In the final phase, erosion and weathering are throttled by flatter topography. We conclude that orogeny acts as a capacitor in the climate system, granting the potential for intense transient CO_2 drawdown when mountain ranges are denuded; the mechanism suggests such a scenario potentially happening 10-50 million years in the future.

Plain Language Summary

Over timescales of tens of millions of years or more, plate tectonics can raise large mountain ranges. CO_2 can be removed from the atmosphere through a complex series of processes involving the weathering of rocks, which depends on processes such as rainfall, which in turn is affected by the presence of mountains. The result is that mountain ranges are associated with a reduction of atmospheric CO_2 and global cooling on these very long timescales. An analysis of geological data suggests a multimillion-year delay between peaks in mountain range uplift at low latitudes and the maximum extent of glaciation over the last 400 million years. Our manuscript explains the delay using two numerical or computer models: a climate and circulation model, and a geochemical model that simulates weathering processes. We show that weathering, and the implied reduction of atmospheric CO_2, happens most intensely

when mountain ranges are eroded, because the ability of weathering to remove CO_2 depends not just on precipitation, but also on the temperature of river runoff. Our mechanism intriguingly suggests such a scenario potentially happening 10-50 million years in the future associated with projected changes to the height of the Tibetan plateau.

1. Introduction

Over geological timescales, atmospheric CO_2 concentration is stabilized by a negative feedback in which the higher temperatures and precipitation associated with higher CO_2 increase the weathering rate of silicate rocks, ultimately forming marine sedimentary carbonates which sequester atmospheric CO_2 (Raymo and Ruddiman, 1992; Maher and Chamberlin, 2014; Walker et al., 1981). The stable concentration of CO_2 is the result of a balance between the tectonic input rate of CO_2 and its removal by silicate weathering (Berner, 2004), and it is broadly understood that changes in CO_2 concentration on timescales of 1-100 Myr over the Phanerozoic Eon (the last 541 million years) have been driven by both variation in CO_2 degassing rates and the amplification of silicate weathering due to changes in paleogeography, lithology and biotic enhancements (Berner, 2004; Royer, 2014; Godderis et al., 2014).

The record of Phanerozoic glaciation shows distinct 'icehouse' periods in which abundant glacial debris are found (Fig. 1 blue bars). For the majority of these icehouse events, the polar 'ice line' (e.g. ice cap terminal latitude) has been at > 60°, while for two major events the ice line has advanced to ≤ 40°. The first of these events lasts for approximately 10 Myrs and occurs at the apex of the Late Paleozoic Ice Age (LPIA) at approximately 290-300 Myr (Isbell et al., 2012; Cather et al., 2009), while the second is occurring during the present Cenozoic Icehouse. The relatively short duration of these major

events is difficult to explain via changes in the CO_2 input rate, which typically happen over a much longer timeframe (e.g. McKenzie et al., 2016).

Glaciation during the LPIA and late Cenozoic have both been linked to low-latitude mountain building events- the Hercynian and Himalayan orogenies respectively (Raymo and Ruddiman, 1992; Godderis et al., 2017) - and in both cases there is a clear relationship over many 10s of Myr between mountain building at low latitudes, low CO_2 and cold climate (Fig. 1). However, on shorter timescales, it is not clear that either major phases of glaciation or lowest levels of CO_2 correspond directly to the uplift of low-latitude mountains. Rather, there is a suggestion that that major phases of glaciations lag behind the maximum extents of high low-latitude mountains by some 10-30 Myrs. Fig. 1A shows a compilation of atmospheric CO_2 estimates using paleosol isotope measurements from the database of Royer (2014), updated in 2017 to include more recent records (Montanez et al., 2016). It shows that the major ice line advance during the LPIA (Isbell et al., 2012) and the minimum in CO_2 concentration occur at 300-290 Ma, in the Early Permian (Fig. 1A), whereas digital elevation models (Scotese and Wright, 2018) and geological assessments (Lardeaux et al., 2001) estimate maximum Hercynian range elevation approximately 20-30 Myr earlier, at around 320 Ma. $^{87}Sr/^{86}Sr$ ratios (McArthur et al., 2012) and global sediment abundance (Hay et al., 2006) also suggest a maximum in global erosion at 320 Ma. Additionally, there is a suggestion that an initial minimum in CO_2 concentration at 330 Ma actually precedes maximum mountain extent. It should be noted that while proxy CO_2 measurements are inherently uncertain, the qualitative trend of CO_2 decline from ~320 to 300 Ma is clearly defined beyond this uncertainty (Montanez et al., 2016).

A similar pattern might be inferred over the Cenozoic, although the ongoing nature of glaciation and mountain building, combined with biases that occur when quantifying erosion rates in the immediate geological past (Willenbring and von Blanckenburg, 2010) make assessment of the present orogenic cycle difficult. Nevertheless, current peak glaciation and low CO_2 in the Cenozoic do appear to lag significantly behind the peak in low-latitude mountain uplift (Scotese and Wright, 2018; Verard et al., 2015) (See Fig 1). Due to uncertainties in reconstructions and proxies, the precise relationship between the timing of mountain uplift and low-latitude glaciation cannot be proven conclusively. Nevertheless, we suggest that there is sufficient inconsistency between records of low-latitude mountain building, CO_2 concentration and severe icehouse climates to require a more detailed investigation of how an orogenic cycle affects the key processes that control weathering, especially for what such an investigation may imply for weathering rates and CO_2 concentration in the next few 10s of Myrs, since the long term future is of great interest to those studying more general aspects of planetary habitability, such as the life span of the biosphere, which has potential implications for the abundance of complex life in the galaxy (e.g. Rushby et al., 2018).

Chemical weathering cannot occur without material supply from physical erosion, as is demonstrated in slowly-eroding, transport-limited catchments (West et al., 2005), and approximately half of present-day chemical weathering occurs in and around rapidly-eroding mountainous areas (Gaillardet et al., 1999; Hilley and Porder, 2008). Silicate weathering rates are variably dependent on local temperature, runoff rate and degree of soil shielding (or depth of the weathering zone). Physically-based equations for estimating silicate weathering at the catchment scale have been derived, validated against field data (West et al., 2005; Gabet and Mudd, 2009; West, 2012), and applied to present day climate (Hartmann et al., 2014), as well

as palaeoclimate models having resolutions of approximately 5-7.5° in the horizontal (Godderis et al., 2017), but have not been coupled to higher resolution climate models that better simulate orographic enhancement of precipitation, and hence changes in hydrology, over an individual orogenic cycle. In addition, it has been assumed previously that physical erosion is a strong control on chemical weathering rates in mountainous areas (Godderis et al., 2017), whereas observations and theoretical modelling point to this relationship only being important in lowlands (transport limitation) (West et al., 2005; Gabet and Mudd, 2009; West, 2012).

In this paper we identify a mechanism which links mountain building, weathering and CO_2, using the LPIA as a case study. Precipitation, runoff and erosion are enhanced over orography (Maher and Chamberlin, 2014; West 2012), but chemical weathering is limited by lower temperatures at high altitudes (Reibe et al., 2004), resulting in three distinct phases for chemical weathering: an increase as mountain building occurs; a decrease when mountain height rises beyond a certain level; an increase to its highest level 10s of Myr after peak topographic height, when mountains have been somewhat denuded, providing a significant source of erodible material, and higher runoff temperature, whilst still allowing elevated precipitation. The resulting effect on CO_2 is to produce two dips in concentration – before and after peak topographic height, with the latter dip being the significantly more pronounced one which can allow low-latitude glaciation.

We demonstrate the proposed mechanism using a combination of physical climate and geochemical models. The physical climate is represented by the IGCM4 (Joshi et al., 2015), which simulates the large-scale global atmospheric circulation and hydrological cycle, and has been extensively employed in studies of present-day tropical circulation and climate

(see supporting information for more details). The IGCM4 has a horizontal resolution of 64x128 ('T42'), exceeding the 40x48 ('R15') resolution of FOAM, which has previously been applied to weathering during the LPIA (Godderis et al., 2017). The IGCM4 also performs well when compared to present day observed precipitation, as shown in the supporting information. The model is set up in three configurations (denoted S, M, H, for short, medium, high), each with paleogeography broadly representative of the Permo-Carboniferous (Scotese and Wright, 2018) (~300 Ma) (Supplementary Fig. S1), as this is the clearest example of a single low-latitude orogeny. The only difference between each configuration is that the maximum height of the mountain range is varied to represent different states of denudation, with the highest being consistent with previous work (Godderis et al., 2017), while the continental configuration remains constant. The present work is therefore isolating the effects of mountain range height on weathering, rather than reconstructing climate history at this time, as was done in Godderis et al. (2017). The ocean model is a so-called q-flux slab.

Each configuration is run for a variety of CO_2 levels. Silicate weathering rates associated with the changes in climate during an orogenic cycle are parameterized using the model of West (2012) which takes runoff volume and temperature from the IGCM4. The weathering model uses physically-based parameterizations of the combined effects of local temperature, runoff and erosion rates to estimate the chemical silicate weathering rate. We choose this model as, with appropriate parameter choices, it has been shown to fit a broad range of catchment data (West, 2012; Maffre et al. 2018), and we further validate it here against a compilation of present day major world rivers (Gaillardet et al., 1999) (see SI). Erosion rates are calculated from local elevation using a previously derived global

relationship (Montgomery and Brandon, 2002), which relates the erosion rate to mean local relief (see SI). See supporting information for more details of both models.

2. Results

Fig. 2 shows time-averaged precipitation and surface temperature from the IGCM4 in runs H, M and S over the land surface at low latitudes. In all three cases, a band of intense precipitation can be seen at low latitudes, which is analogous to the present-day inter-tropical convergence zone (ITCZ). While the amount of precipitation over the ocean is similar in all cases, the precipitation over land varies very strongly according to the height of the topography. Runs H and M (Figs. 2A and 2B) have intense precipitation over land peaking above 10 mm day^{-1} on the flanks of the mountains, while Run S (Fig. 2C) has a much weaker and broader band of land precipitation, peaking at 3 mm day^{-1} away from the coasts. The most intense precipitation falls on the flanks of the mountains, where the surface temperature is far lower than the sea-level value; in run H, the most intense precipitation falls onto a surface that is up to 20 K colder than in run S (Figs. 2B and 2F), while in run M the intense band of precipitation is in an area that is up to 10 K colder than in run S (Figs. 2D and 2F).

The differences in precipitation and temperature lead to differences in runoff and chemical weathering. Our model run for High mountains (H) has relatively low surface evaporation at the location of the precipitation band because it lies at higher, colder altitudes than in run M, meaning that the remaining runoff is higher (Figs. 3A and 3C). However, Figs. 3B and 3D show a clear increase in total silicate weathering flux from case H to case M (i.e. mountain denuding) of ~20-50%, despite decreases in both runoff and erosion associated with mountain height. In other words, the effect of higher temperature in run M dominates the weathering response. As expected, run S displays even lower rainfall (Fig. 2E) and a

higher surface temperature, leading to more evaporation, reduced runoff and reduced chemical and physical weathering (Fig. 3E). The difference in weathering between runs M and H might in reality be enhanced further by very high erosion rates actually inhibiting weathering (Gabet and Mudd, 2009).

The global implications of these results are examined in Fig. 4A, which shows globally integrated weathering rates for the different IGCM runs against atmospheric CO_2 concentration. There is a clear non-monotonic relationship between weathering and orography: the largest weathering rates for a given CO_2 concentration are in case M for all values of pCO_2 (purple line). Fig. 4B shows the estimated stable level of atmospheric CO_2 for a fixed estimate of the assumed global weathering flux required to balance degassing (taken as 1.2×10^8 t yr^{-1}), and schematic arrows showing when the key geophysical, climatic and chemical processes are maximized as the mountain range is eroded away. Equilibrium CO_2 is around ~550 ppmv at maximum mountain height (i.e. case H), and is reduced to ~250 ppmv after partial denudation (case M), before increasing back to ~500 ppmv once mountains are denuded completely (case S). This behavior is consistent with the dynamics of CO_2 concentration between ~320 and ~290 Ma (Royer, 2014; Montanez et al., 2016), during the initial denudation of the Hercynian range.

3. Discussion

Whether peak chemical weathering precedes or lags behind peak erosion depends on differences in weathering between mountain uplift and denudation periods. Three mechanisms suggest that the former phase permits less integrated chemical weathering than the latter. Firstly, the latter is simply longer-lasting than the former (Abbott et al., 1997),

although it should be noted that uplift timescales are still sufficiently long to allow the silicate weathering feedback to equilibrate atmospheric CO_2. Secondly, when weathering is kinetically limited (i.e. physical weathering > chemical weathering), there must be accumulation of physically weathered material in the system, either as mobile regolith or as sedimentary deposits (Gabet and Mudd, 2009; Hilley et al., 2010), some of which will be available for subsequent chemical weathering. This contrasts with initial uplift where surface terrains are more likely to need physical erosion before fresh material is available to be weathered. Furthermore it has been suggested that in such old surfaces, weathering is also inhibited by greater regolith thickness (Goudie and Viles, 2012). When fresh surface is finally exposed, the steep, 'spiky' terrain that emerges may strongly limit silicate weathering, due to very high erosion rates, and favor dissolution of carbonate rather than silicate minerals, leading to no net long term CO_2 drawdown (Goudie and Viles, 2012). Thirdly, whilst glaciers may lead to enhanced weathering through scour related processes (Anderson et al., 1997), large ice caps will tend to suppress weathering, while retreating glaciers may lead to enhanced carbonate and silicate weathering of glacial deposits (Anderson et al., 1997; Kump and Alley, 1994), suggesting that the net effect of glaciation of high mountains is to pause chemical weathering whilst accumulating weatherable material.

Fig. 1 does strongly suggest that prior to both of the deep glaciations considered here, there is an earlier period of CO_2 drawdown, coincident with initial uplift, but less severe than that following ~20 Myr after peak mountain height, with a rebound of CO_2 in between, associated with the period of peak mountain height. This is consistent with the idea that peak weathering will happen at intermediate erosion rates (Carretier et al., 2014) but the potential for chemical weathering and thus deep glaciation is greater as mountains denude. Present day

global erosion rates in tectonically inactive regions are around 0.1 mm yr^{-1} (Montgomery and Brandon, 2002), implying 1000m of mountain eroded over a timeframe of ~10 Myr. Although the Tibetan Plateau lies at a higher latitude than the LPIA-era Hercynian range, the intense monsoonal precipitation (and weathering) associated with this range is important when considering global weathering (see supplementary Fig. S6). It is therefore possible that in the next 10-50 Myr the erosion of the Himalayas, and associated discharge of the weathering capacitor, may overwhelm the negative feedbacks in the global carbon cycle, causing a severe icehouse period to develop in a similar manner to the LPIA.

We conclude that a delayed, climate-controlled capacitor may have allowed low-latitude mountain building to store weatherable silicates at high altitudes which are later discharged, greatly reducing atmospheric CO_2 concentrations, and establishing 'icehouse' climates for periods of several 10s of Myrs. The conceptual picture (see Fig. 4B) can explain the potential inconsistency between periods of low-latitude mountain building in the geological record and CO_2 drawdown (see Fig.1). It also suggests that CO_2 drawdown may proceed in a transient pulse having a non-monotonic dependence on mountain height, explaining why such events are difficult to replicate in current zero-dimensional biogeochemical models (Berner, 2006; Bergman et al., 2004). Datasets with enhanced time-resolution on these long timescales are needed in order to test this hypothesised mechanism. Whilst our results are most directly applicable to the LPIA, it is possible that future discharge of the weathering capacitor may cause a similar icehouse period to develop in the next 10-50 Myr.

References

Abbott, L. et al. (1997) Measurement of tectonic surface uplift rate in a young collisional mountain belt. *Nature* **385**, 501-507.

Anderson, S., Drever, J. & Humphrey, N. (1997) Chemical weathering in glacial environments. *Geology* **25**, 399.

Bergman, N., Lenton, T. & Watson, A. (2004) COPSE: A new model of biogeochemical cycling over Phanerozoic time. *American Journal of Science* **304**, 397-437.

Berner, R. (2004) *The phanerozoic carbon cycle*. (Oxford University Press).

Berner, R. (2006) GEOCARBSULF: A combined model for Phanerozoic atmospheric O2 and CO2. *Geochimica et Cosmochimica Acta* **70**, 5653-5664.

Carretier, S., Godderis, Y., Delannoy, T. & Rouby, D. (2014) Mean bedrock-to-saprolite conversion and erosion rates during mountain growth and decline. Geomorphology 209, 39-52.

Cather, S. M., Dunbar, N. W., McDowell, F. W., McIntosh, W. C. & Scholle, P. A. (2009) Climate forcing by iron fertilization from repeated ignimbrite eruptions: The icehouse–silicic large igneous province (SLIP) hypothesis. *Geosphere* **5**, 315-324.

Gabet, E. & Mudd, S. (2009) A theoretical model coupling chemical weathering rates with denudation rates. *Geology* **37**, 151-154.

Gaillardet, J., Dupré, B., Louvat, P. & Allègre, C. (1999) Global silicate weathering and CO2 consumption rates deduced from the chemistry of large rivers. *Chemical Geology* **159**, 3-30.

Goddéris, Y., Donnadieu, Y., Le Hir, G., Lefebvre, V. & Nardin, E. (2014) The role of palaeogeography in the Phanerozoic history of atmospheric CO2 and climate. *Earth-Science Reviews* **128**, 122-138.

Godderis, Y. *et al*. (2017) Onset and ending of the late Palaeozoic ice age triggered by tectonically paced rock weathering, *Nature Geoscience* **10**, 382–386.

Goudie, A. and Viles, H. (2012) Weathering and the global carbon cycle: Geomorphological perspectives. *Earth Science Reviews* **113**, 59-71.

Hartmann, J., Moosdorf, N., Lauerwald, R., Hinderer, M. & West, A. (2014) Global chemical weathering and associated P-release — The role of lithology, temperature and soil properties. *Chemical Geology* **363**, 145-163.

Hay, W. et al. (2006) Evaporites and the salinity of the ocean during the Phanerozoic: Implications for climate, ocean circulation and life. *Palaeogeography, Palaeoclimatology, Palaeoecology* **240**, 3-46.

Hilley, G. E. & Porder, S. (2008) A framework for predicting global silicate weathering and CO2 drawdown rates over geologic time-scales. *Proc. Nat. Academy. Sci.* **105**, 16855–16859.

Hilley, G., Chamberlain, C., Moon, S., Porder, S. & Willett, S. (2010) Competition between erosion and reaction kinetics in controlling silicate-weathering rates. *Earth and Planetary Science Letters* **293**, 191-199.

Isbell, J. L. *et al.* (2012) Glacial paradoxes during the late Paleozoic ice age: Evaluating the equilibrium line altitude as a control on glaciation. *Gondwana Research* **22**, 1-19.

Joshi, M., Stringer, M., van der Wiel, K., O'Callaghan, A. & Fueglistaler, S. (2015) IGCM4: a fast, parallel and flexible intermediate climate model. *Geoscientific Model Development* **8**, 1157-1167.

Kump, L. & Alley, R. (1994) in *Material Fluxes on the Surface of the Earth* (National Academy Press).

Lardeaux, J. M., Ledru, P., Daniel, I. & Duchene, S. (2001) The Variscan French Massif Central– a new addition to the ultra-high pressure metamorphic 'club': exhumation processes and geodynamic consequences. *Tectonophysics* **332**, 143-167.

Maffre, P., Ladant, J-B., Moquet, J-S., Carretier, S., Labat, D., Goddéris, Y. (2018) Mountain ranges, climate and weathering. Do orogens strengthen or weaken the silicate weathering carbon sink? *EPSL* **493,** 174-185.

Maher, K. & Chamberlain, C. (2014) Hydrologic Regulation of Chemical Weathering and the Geologic Carbon Cycle. *Science* **343**, 1502-1504.

McArthur, J.M., Howarth, R.J., Shields, G.A. (2012) Chapter 7 - Strontium Isotope Stratigraphy, the Geologic Time Scale. Elsevier, Boston, pp. 127–144.

McKenzie, N. et al. (2016) Continental arc volcanism as the principal driver of icehouse-greenhouse variability. *Science* **352**, 444-447.

Montañez, I. P. *et al.* (2016) Climate, pCO2 and terrestrial carbon cycle linkages during late Palaeozoic glacial–interglacial cycles. *Nature Geoscience* **9**, 824-828.

Montgomery, D. & Brandon, M. (2002) Topographic controls on erosion rates in tectonically active mountain ranges. *Earth and Planetary Science Letters* **201**, 481-489.

Moon, S. C. P. Chamberlain, G. E. Hilley (2014) New estimates of silicate weathering rates and their uncertainties in global rivers. Geochimica et Cosmochimica Acta 134, 257–274.

Raymo, M. & Ruddiman, W. Tectonic forcing of late Cenozoic climate (1992) *Nature* **359**, 117-122.

Riebe, C., Kirchner, J. & Finkel, R. (2004) Sharp decrease in long-term chemical weathering rates along an altitudinal transect. *Earth and Planetary Science Letters* **218**, 421-434.

Royer, D. (2014) in *Treatise on Geochemistry, Volume 6: The Atmosphere - History* (Farquhar, J.ed.) 251-267 (Elsevier).

Rushby, A. J., Johnson, M., Mills, B. J. W., Watson, A. J. & Claire, M. W. (2018) Long-Term Planetary Habitability and the Carbonate-Silicate Cycle. *Astrobiology* **18**, 469-480.

Scotese, C.R. & Wright, N. (2018) PALEOMAP Paleodigital Elevation Models (PaleoDEMS) for the Phanerozoic. *Earthbyte*. https://www.earthbyte.org/paleodem-resource-scotese-and-wright-2018/

Van Der Wiel, K., Matthews, A., Joshi, M. & Stevens, D. (2016) Why the South Pacific Convergence Zone is diagonal. *Climate Dynamics* **46**, 1683-1698.

Vérard, C., Hochard, C., Baumgartner, P.O., Stampfli, G.M., Liu, M. (2015) 3D palaeogeographic reconstructions of the Phanerozoic versus sea-level and Sr-ratio variations. *Journal of Palaeogeography* **4**, 64-84.

Walker, J., Hays, P. & Kasting, J. (1981) A negative feedback mechanism for the long-term stabilization of Earth's surface temperature. *Journal of Geophysical Research* **86**, 9776.

West, A., Galy, A. & Bickle, M. (2005) Tectonic and climatic controls on silicate weathering. *Earth and Planetary Science Letters* **235**, 211-228.

West, A. J. (2012) Thickness of the chemical weathering zone and implications for erosional and climatic drivers of weathering and for carbon-cycle feedbacks. *Geology* **40**, 811-814.

Willenbring, J. K. & Blanckenburg, F. v. (2010) Long-term stability of global erosion rates and weathering during late-Cenozoic cooling. *Nature* **465,** 211-214.

Acknowledgements

We acknowledge the support of resources provided by the High Performance Computing Cluster supported by the Research and Specialist Computing Support service at the University of East Anglia. We acknowledge UK Natural Environment Research Council (NERC) grants. BJWM acknowledges a University of Leeds Academic Fellowship.

Author Contributions

All authors contributed to devising the study, analysis and manuscript writing. M Joshi prepared and performed IGCM simulations, B Mills performed weathering rate calculations.

Competing Interests

There are no competing interests.

Data Availability

Relevant model output placed in an institutional repository at the University of East Anglia: https://people.uea.ac.uk/en/datasets/search.html

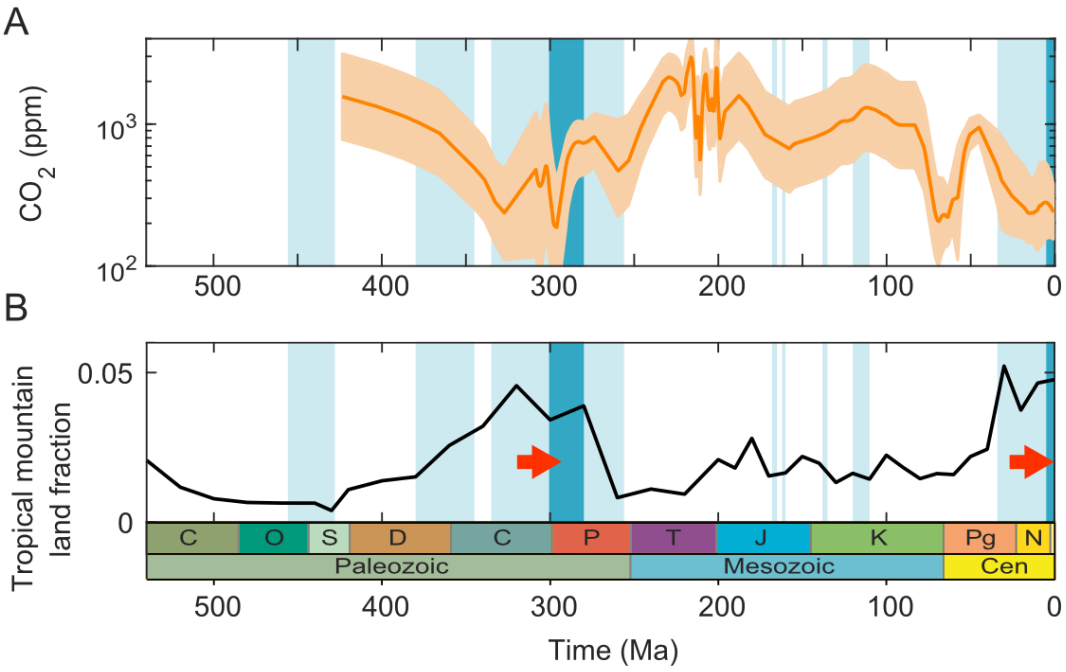

Fig. 1. CO_2, glaciation and low-latitude mountains. Proxy atmospheric CO_2 from combined paleosol measurements (Royer, 2014; Montanez et al., 2016), with uncertainty determined as 16^{th} and 84^{th} percentiles (A), timeline of fraction of 30°N-30°S land above 1km elevation (Scotese and Wright, 2018) (B). Both timelines are shown against glacial periods as blue bars (as compiled by Cather et al., 2009), the dark blue representing the most severe glaciation where ice caps reached 40° of latitude. The thick red arrows represent the estimated delay between maximum elevation and maximum glaciation.

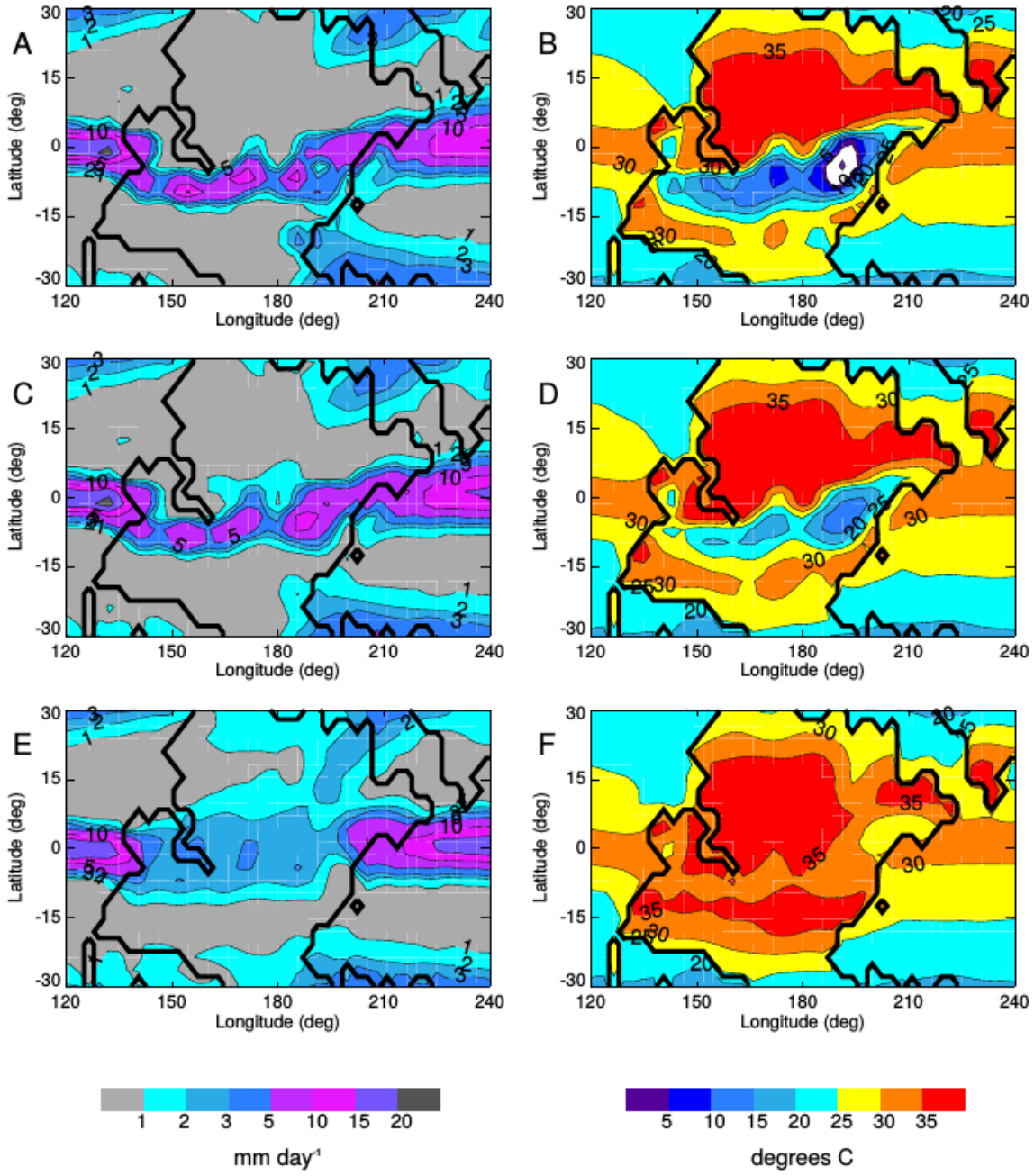

Fig. 2. Time-averaged climate in three IGCM4 runs: H (panels A, B), M (panels C, D), S (panels E, F). (A, C, E) are Precipitation (mm day^{-1}); (B, D, F) are Surface temperature (°C). The land-ocean boundary is shown by the thick black contour.

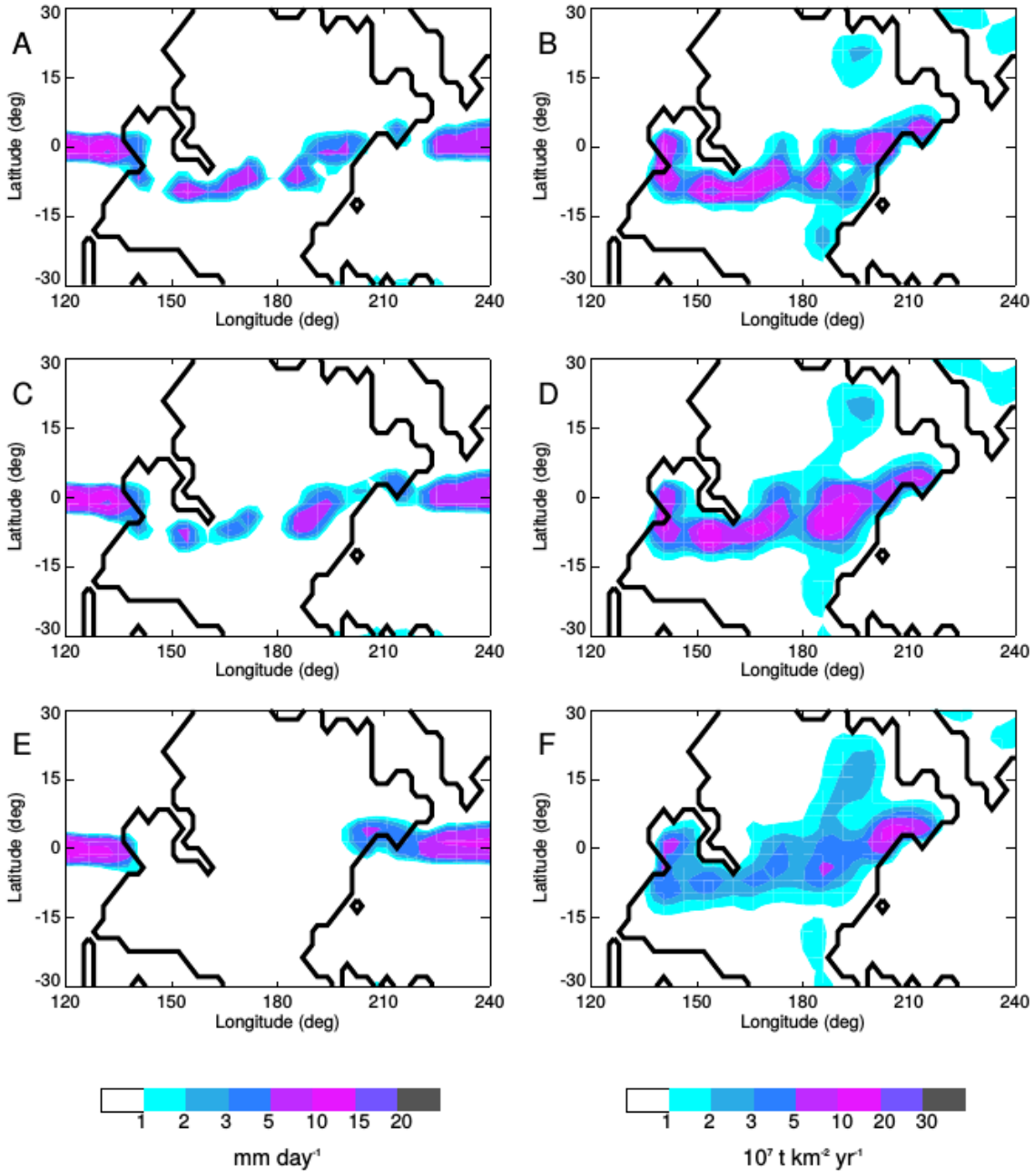

Fig. 3. Time-averaged surface hydrology in three IGCM4 runs: H (panels A, B), M (panels C, D), S (panels E, F). (A, C, E) are Precipitation minus Evaporation (mm day^{-1}); (B, D, F) are total silicate weathering (10^7 t km^{-2} yr^{-1}) over land. The land-ocean boundary is shown by the thick black contour.

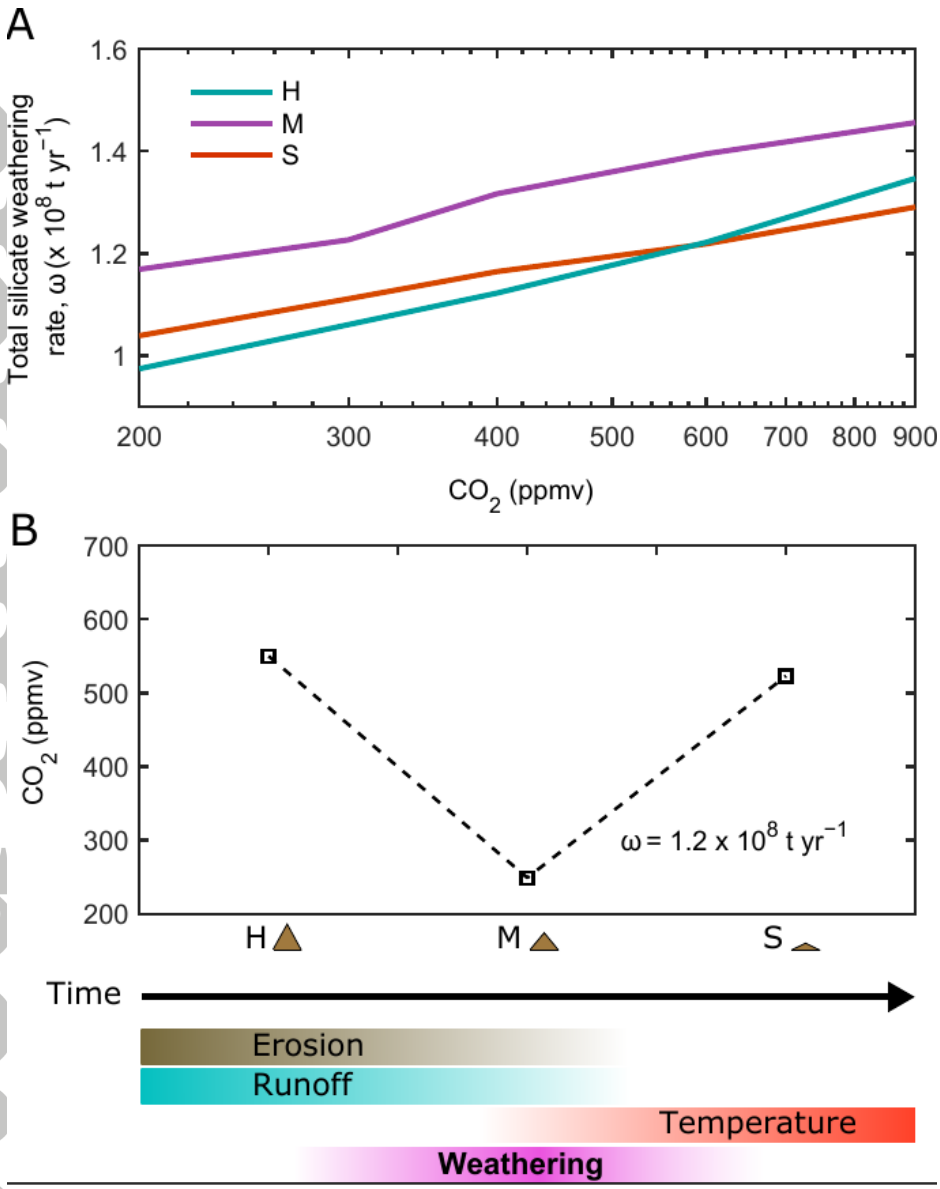

Fig. 4. (A) Global chemical weathering rate (in units of 18^8 t yr^{-1}) vs CO_2 inferred from the weathering model forced by IGCM output (see Methods in supporting information). The mountain configurations are H (blue), M (purple) and S (orange). (B) Timeline of CO_2 concentration required for atmospheric stability assuming a required weathering rate of $1.2x10^8$ t yr^{-1} in the "denudation" phase, as the mountain range is eroded from H, through M, to S. The coloured bars beneath panel B show where runoff (blue), erosion (brown), and runoff temperature or potential chemical weathering (red) are maximised, causing a maximum in total weathering and CO_2 drawdown (purple).